Applied Catalysis B: Environmental 92 (2009) 194–201

Contents lists available at ScienceDirect

Applied Catalysis B: Environmental

journal homepage: www.elsevier.com/locate/apcatb

Manganese and iron oxides as combustion catalysts of volatile organic compounds

Flavia G. Durán [a,*], Bibiana P. Barbero [a], Luis E. Cadús [a], Cristina Rojas [b], Miguel A. Centeno [b], José A. Odriozola [b]

[a] Instituto de Investigaciones en Tecnología Química (INTEQUI), UNSL-CONICET, Casilla de correo 290,5700 San Luis, Argentina
[b] Instituto de Ciencia de Materiales de Sevilla, Centro Mixto CSIC-Universidad de Sevilla, Avda Americo Vespuccio s/n, 41092 Sevilla, Spain

ARTICLE INFO

Article history:
Received 9 March 2009
Received in revised form 3 July 2009
Accepted 13 July 2009
Available online 18 July 2009

Keywords:
Iron-based catalyst
Manganese-based catalyst
VOCs
Ethanol
Toluene
Ethyl acetate
Catalytic combustion

ABSTRACT

FeMn mixed oxides were prepared by the citrate method with Fe:Mn atomic ratio equal to 1:1, 1:3 and 3:1. The sample was characterized by means of specific surface area measurements, X-ray diffractometry (XRD), temperature programmed desorption of oxygen (O_2-DTP), temperature programmed reduction (TPR), X-ray fluorescence (XRF), transmission electron microscopy (TEM and SAED) and high resolution TEM (HREM). The characterization results demonstrated the formation of a Mn_2O_3–Fe_2O_3 solid solution. The catalytic performance in ethanol, ethyl acetate and toluene total oxidation on these samples was better than on Fe_2O_3 and Mn_2O_3 pure oxides.

1. Introduction

Total catalytic oxidation technology is widely used in several industrial processes for air pollution abatement, especially for control of volatile organic compound emissions. Compared with thermal combustion techniques, higher efficiencies at lower operating temperatures are reached, obtaining considerable environmental and economic benefits.

The manganese oxides including bulk MnO_2, Mn_2O_3 and Mn_3O_4, as well as those supported on carriers such as silica, alumina, titania and zirconia [1–3] are a cheaper alternative in environmental catalysis. Zaki et al. [4] have shown that MnO_2 decomposition in oxidizing (O_2, air) and non-oxidizing (N_2) gas atmospheres starts at 550–600 °C and results eventually, in the formation of Mn_3O_4. The decomposition course of MnO_2 into Mn_3O_4 is mediated by the formation and decomposition of Mn_5O_8 and subsequently Mn_2O_3. This Mn_2O_3 is a stable phase. MnO_x is capable of mobilizing electrons and, thus, of generating the mobile-electron environment required by redox catalysts. Mn_2O_3 can absorb oxygen and act, in an oxidizing atmosphere, like p-type semiconductors. This is due to the possibility of Mn cation to reach the tetravalent state. An n-type semiconductor; like Fe_2O_3; cannot be further oxidized. Baldi et al. [5] have prepared Mn_2O_3–Fe_2O_3 mixtures by co-precipitation of manganese acetate and iron nitrate in ammonium carbonate aqueous solution. After the ageing, the precipitated fraction was filtered, dried and calcined at 1073 K for 3 h. The authors showed that these materials are active catalysts for the catalytic oxidation of propane and propene at low temperatures. They proposed synergy between iron and manganese oxide components. The phase diagram for Mn–Fe–O system has been published by Kedesdy and Tauber [6]. The formation of several arrangements such as solid solution or $Fe_xMn_yO_4$ spinels has been proposed. It has also been observed that transition metals such as Mn, in the spinel lattice can strongly modify the redox properties of the ferrites and thus influence on their stability. Guillemet-Fristch et al. [7] have shown that redox reactions and other factors may play an even more stabilizing role in the spinels than in the binary oxides. The physico-chemical properties of the ferrites are strongly dependent on the site, nature and amount of the metal incorporated in the structure. From the phase diagram of the Fe_2O_3–Mn_2O_3 system as reported in the literature [6], a single phase $(Mn_{1-y}Fe_y)_2O_3$ material would be expected. Mn_3O_4 phase is formed in a flow of hot air and transformed into Mn_2O_3 at approximately 600 °C. Mn_2O_3 is transformed again into Mn_3O_4 at

* Corresponding author at: Instituto de Investigaciones en Tecnología Química (INTEQUI), UNSL-CONICET, Casilla de correo 290,5700 San Luis, Argentina. Fax: +54 2652 426711.
E-mail address: fduran@unsl.edu.ar (F.G. Durán).

0926-3373/$ – see front matter © 2009 Elsevier B.V. All rights reserved.
doi:10.1016/j.apcatb.2009.07.010

high temperatures. Fe_2O_3–Mn_2O_3 solid solution is associated with a change in the cubic structure of Mn_2O_3 phase. The solid solution evolves at high temperature and the lattice constant diminishes due to the difference between the ionic rations of Mn^{3+} and Fe^{3+}. At high temperature, great amounts of Mn^{3+} are replaced by Fe^{3+} ions which are smaller.

In this work, we synthesise catalysts with different Fe/Mn atomic ratios by means of the citrate method. The aim of this work is to study in detail the phase composition, texture and other structural and physico-chemical characteristics, and to correlate them with the catalytic activity in oxidation reactions.

2. Experimental

2.1. Catalyst preparation

FeMn oxide catalysts with Fe:Mn atomic ratio equal to 1:1, 1:3 and 3:1 were prepared by the citrate method $Mn(NO_3)_2{\cdot}4H_2O$ (Fluka 97%), $Fe(NO_3)_3{\cdot}9H_2O$ (Mallinckrodt, 98%) and citric acid (Merck, 99.5%) were used as reagents. An aqueous solution of citric acid with a 10% excess over the equivalents of cations was prepared. The aqueous solutions of metal nitrates were added to that of citric acid, and agitated for 15 min. The resulting solution was concentrated by slowly evaporating water under vacuum in a rotavapor at 50 °C until a gel was obtained. This gel was dried in an oven, at 120 °C overnight in order to produce a solid amorphous citrate precursor. The resulting precursor was milled and then calcined in air at 500 and 650 °C for 3 h. The resulting catalysts were denoted as: FeMn *X*:*YT* where *X*:*Y* = 1:1, 1:3 or 3:1 represents the Fe:Mn atomic ratio and *T* = 500 or 650 °C. An artificially mechanical mixture was prepared. A 1:1 Mn_2O_3–Fe_2O_3 mechanical mixture with Fe:Mn atomic ratio equal to 1:1 was prepared as follows: commercial Fe_2O_3 powder (Fluka) and Mn_2O_3 obtained by thermal decomposition of manganese carbonate (Fluka) were milled in a Fritsch ball mill operated intermittently with a magnitude of 1.5 for 24 h, and then calcined in air at 500 °C for 3 h.

2.2. Characterization

2.2.1. BET specific surface area

The specific surface area of catalysts was calculated by the BET method from the nitrogen adsorption isotherms at 77 K after outgassing the samples at 250 °C by using a Micromeritics Gemini V apparatus.

2.2.2. X-ray diffraction (XRD)

XRD patterns were obtained by using a Rigaku diffractometer operated at 30 kV and 25 mA by employing V-filtered Cr Kα radiation (λ = 0.2291 nm). The crystalline phases were identified by reference to powder diffraction data.

2.2.3. Temperature programmed desorption of oxygen (O_2-DTP)

O_2-TPD experiments were performed in a quartz reactor using a TCD as detector. In each analysis, 500 mg samples were pre-treated with helium gas increasing the temperature from room temperature up to 500 °C at 10 °C min^{-1}. Then, the samples were oxidized with a 20% O_2/He mixture at a total flow rate of 30 ml min^{-1} at the calcination temperature (500 or 650 °C) for 30 min. Afterwards, they were cooled down to room temperature and flushed by a stream of purified He for 30 min. The desorption was carried out in the same conditions as the pre-treatment, maintaining the temperature at 500 °C until the TCD signal returned to baseline.

2.2.4. Temperature programmed reduction (TPR)

The TPR was performed in a quartz U-type tubular reactor using a TCD as detector. A 40 mg sample was used. The reducing gas was a mixture of 5 vol.% H_2/N_2, at a total flow rate of 30 ml min^{-1}. The temperature was increased at a rate of 10 °C min^{-1} from room temperature to 700 °C; then, it was kept constant at 700 °C until the signal of hydrogen consumption returned to the initial values.

2.2.5. X-ray fluorescence (XRF)

The composition of every sample was determined by X-ray fluorescence on a PW 1400 Philips instrument. The calibration was made by using patterns prepared with known amounts of Fe_2O_3 and Mn_2O_3.

2.2.6. TEM

Transmission electron microscopy (TEM and SAED) and high resolution TEM (HREM) studies were performed with a Philips CM200 and with a JEOL 2000EX, having 0.23 nm and 0.21 nm point-to-point resolution, respectively. The chemical composition and homogeneity were studied with an EDX detector D-X4 coupled to the Philips CM200. For these studies, a suspension of the samples in ethanol was placed on a holey-carbon grid.

2.2.7. Catalytic test

The catalysts were evaluated in total oxidation of ethanol, ethyl acetate and toluene using a quartz reactor of fixed bed. The catalyst powder was pressed, crushed and sieved to a size of 20–35 mesh (0.5–0.85 mm) for the catalytic evaluation and then, a 300 mg sample was diluted with 1.5 g glass of the same size as that of the catalyst. The reaction mixtures (100 ml min^{-1}) were C_2H_5OH:O_2:He = 1:20:79 molar ratio and $C_4H_8O_2$:O_2:He = 1:20:79 molar ratio. The temperature, measured with a coaxial thermocouple, varied between 80 and 270 °C, increasing in steps of 20 and 5 °C for ethanol oxidation and 150 and 300 °C, in steps of 10 and 5 °C, for ethyl acetate oxidation. The data reported at each reaction temperature were the average of at least two steady-state measurements. The reagents and products of reaction were analyzed on line by using two GC equipment: a Shimadzu GC-8A with a Carbosphere column in order to separate O_2 and CO_2 and a Buck Scientific 910 with a Carbowax 20/Chromosorb W column in order to separate the VOCs.

3. Results and discussion

The results of catalytic activity in ethanol, ethyl acetate and toluene oxidation are shown in Table 1. Taking into account the nominal composition and T_{50} as parameter for comparing the catalytic performance it is observed that every FeMn mixed catalyst shows a better performance than that expected from the contribution of the pure oxides. The catalysts calcined at 500 °C are more active than Mn_2O_3 which has been reported as a good catalyst in total combustion of VOCs. There is a difference of T_{80}

Table 1
Catalytic activity in ethanol and ethyl acetate oxidation for Fe_2O_3, Mn_2O_3, FeMn 1:1; FeMn 1:3 and FeMn 3:1 catalyst. Catalysts weight: 300 mg. Total volumetric flow (F_{vt}) = 100 ml min^{-1}. Feed composition: C_2H_5OH:O_2:He = 1:20:79. Total volumetric flow (F_{vt}) = 100 ml min^{-1}. Feed composition: C_4H_8OH:O_2:He = 1:20:79.

Catalyst	Ethanol		Ethyl acetate		Toluene
	T_{50} (°C)	T_{80} (°C)[a]	T_{50} (°C)	T_{80} (°C)[a]	T_{80} (°C)[a]
Fe_2O_3	260	314	290	309	365
Mn_2O_3	200	249	252	270	296
FeMn 1:1500	150	219	227	245	293
FeMn 1:3500	165	223	240	256	282
FeMn 3:1500	160	230	252	270	307
FeMn 1:1650	180	242	261	275	302
FeMn 1:3650	190	248	255	271	295
FeMn 3:1650	195	256	258	271	293

[a] T_{80} of Y_{CO_2}.

Table 2
Composition from X-ray fluorescence, specific surface areas and XPS.

Catalyst	X-ray fluorescence Fe/Mn	S_{BET} ($m^2\,g^{-1}$)	XPS Fe/Mn atomic ratio
FeMn 1:1500	0.94	85	0.95
FeMn 1:3500	0.34	60	0.31
FeMn 3:1500	3.12	103	–
FeMn 1:1650	0.95	30	0.99
FeMn 1:3650	0.34	23	0.31
FeMn 3:1650	3.19	11	–

(temperature at which the conversion reaches 80%) between FeMn 1:1500 and Mn_2O_3. This difference is 30 and 25 °C for combustion of ethanol and ethyl acetate, respectively. To evaluate these differences in T_{80}, it is important to consider that even in a stream with high composition in VOC, the ΔH of combustion is low with regard to the sensitive heat that the inert needs to reach the reaction temperature.

With the aim to found an explanation to the excellent catalytic performance of FeMn mixed catalysts, a detailed description of the physical and physico-chemical characteristics of the catalysts is presented below.

The relative metal compositions of FeMn catalysts were determined using X-ray fluorescence. The results are shown in Table 2. In all cases, the atomic ratios were very closely to the nominal values. Furthermore, in every zone below 25 nm analyzed by means of EDX, Mn, Fe and O were detected. These analyses also corresponded very closely to nominal composition of FeMn 1:1 T and FeMn 1:3 T catalysts. The composition of FeMn 1:1 T and FeMn 1:3 T catalysts by mapping showed an extremely homogeneous composition. Unlike FeMn 1:1 T and FeMn 1:3 T catalysts, the composition of FeMn 3:1 T catalyst was non-homogeneous.

Extremely homogeneous materials may normally be obtained by the citrate method, furthermore, EDX results may be explained by the formation of a Mn_2O_3–Fe_2O_3 solid solution or a mixed oxide such as spinel phase.

From the phase diagram of the Mn_2O_3–Fe_2O_3 system as reported in the literature by Kedesdy and Tauber [6], it would be expected a solid solution or a single phase β-$(Mn_{1-y}Fe_y)_2O_3$ material. However, the conditions used in this work are different to that reported by Kedesdy and Tauber to obtain $MnFe_2O_4$ and the spinel $(Mn_xFe_{1-x})_3O_4$ is generally obtained in air at temperatures above 1223 K.

Baldi et al. [5] from thermodynamic phase diagram show that below 1173 K, the solubility of Fe_2O_3 into α-Mn_2O_3 is very high although decreasing significantly with decreasing temperature, while the solubility of Mn_2O_3 into α-Fe_2O_3 is always low (less than 10%, w/w). Jaggi et al. [8] have studied the effect of manganese content on the phase composition of iron/manganese catalysts and found that a single phase solid solution of Mn in hematite, α-$(Fe_{1-x}Mn_x)_2O_3$, was formed after calcination at 773 K. The Fe-rich material exists as a single phase solid solution α-$(Fe_{1-x}Mn_x)_2O_3$ whereas the Mn-rich material is a mixture of α-$(Fe_{1-x}Mn_x)_2O_3$ and β-$(Mn_{1-y}Fe_y)_2O_3$.

Fig. 1 shows XRD for FeMn 1:1; FeMn 1:3 and FeMn 3:1 catalysts calcined at 500 °C and 650 °C. XRD for the pure oxides – Mn_2O_3 and Fe_2O_3 – exhibits the typical patterns of α-Mn_2O_3 (bixbyite) and of α-Fe_2O_3 (hematite), respectively. For the bimetallic materials, the X-ray diffractograms of FeMn 1:1 and FeMn 1:3 are very similar to that of α-Mn_2O_3. Only for FeMn 1:1, the more intense diffraction lines corresponding to Mn_3O_4 are observed. Jacobsite, $MnFe_2O_4$ (PDF 38–430), Jacobsite syn. $Mn_{0.6}Fe_{0.4}O_4$ (PDF 88–1965), mixed oxides $Mn_{1.58}Fe_{1.42}O_4$ and $Mn_{0.43}Fe_{2.57}O_4$ (PDF 89–2807 and, 89–2808, respectively) are not detected. It is notable that the bixbyite phase was observed mainly on the catalyst with a Fe:Mn molar ratio of 1:3. Bixbyite phase has

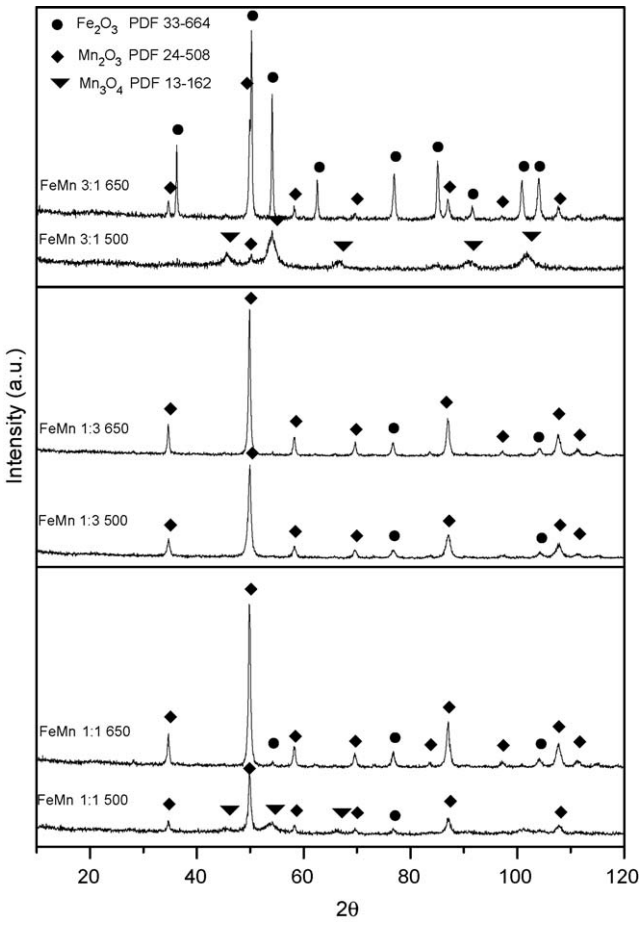

Fig. 1. XRD pattern of FeMn 1:1; FeMn 1:3 and FeMn 3:1 catalyst calcined at 500 and 650 °C.

an empiric formula which may be as follows: $Mn_{1.5}Fe_{0.5}O_3$, $(Fe,Mn)_2O_3$ or $(Fe_{0.63}Mn_{0.37})_2O_3$, all cubic structures with unit cell parameters of $a = 9.365$; $b = 9.400$ and $c = 9.4126$ respectively. Manganese form oxides crystallize in different oxidation states (2+, 3+ and 4+). The more stable manganese oxide is the well-known Mn_2O_3 which exists in two different forms: the stable α-Mn_2O_3 and the meta-stable defect tetragonal spinel γ-Mn_2O_3. The former has an orthorhombically distorted bixbyite structure. Mn_2O_3 is the only sesquioxide having this structure; its origin is thought to lie in the expected substantial Jahn–Teller distortion associated with the d^4 Mn^{3+} ion. For the low temperature form, there are five distinguishable Mn-sites. The average Mn–O distances are 2.003, 2.002, 2.043, 2.043 and 2.042 Å corresponding to α-Mn_2O_3 orthorhombic structure.

The information about the morphology and the phases present in the samples was obtained by TEM, SAED and HREM studies. The indexation of the rings of the SAED patterns obtained for Fe:Mn 1:3500 and Fe:Mn 1:1500 catalysts has been assigned to the bixbyite phase. Fig. 2 shows the electron diffraction obtained for Fe:Mn 1:3500 is shown. The three first rings correspond to the inter-planar spacing of ca. 2.6, 3.6, and 4.6 Å being assigned to the $(\bar{2}\,2\,2)$, $(1\,2\,1)$ and $(0\,2\,0)$ family planes of the bixbyite phase, respectively. The study of the samples by HREM confirms the presence of crystals of the bixbyite phase. For example, in the HREM image of Fig. 3, there is a 2.7 Å distance between fringes, which corresponds to a $(\bar{2}\,2\,2)$ family planes. The inset in this figure is the digital diffraction pattern (DDP) obtained from the encircle crystal in the experimental images. The inter-planar spacing values of 2.7 and 3.8 Å measured for the spot could be assigned to $(\bar{2}\,2\,2)$ and $(1\,2\,1)$ family planes of the bixbyite structure, while the

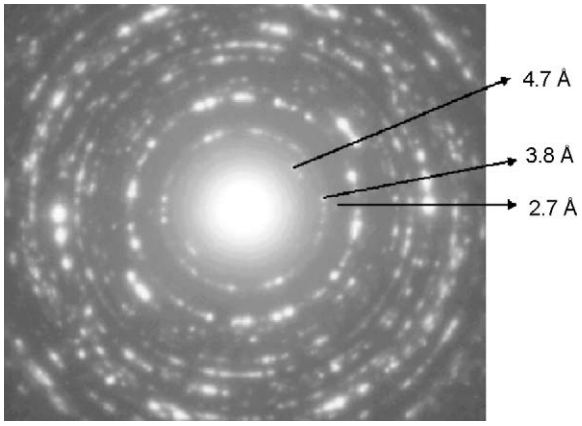

Fig. 2. Electron diffraction obtained for FeMn 1:3500.

geometry of the DDP corresponds to [1 2 3] zone axis. Other orientations such as the [1 3 5] and [1 1 3] zone axes have also been identified during the HREM study. In summary, the HREM characterization of the FeMn 1:1500 and FeMn 1:3500 catalysts indicates in all the cases the formation of the bixbyite phase (cubic or orthorhombic) in which Fe would be placed randomly in substitutional positions of the Mn. Both phases of the bixbyite are similar with a slight change in the lattice parameters and atomic positions. In the cubic structure, there are two positions for manganese while in the orthorhombic structure, there are five. No other crystalline phase is observed either in FeMn 1:1500 or FeMn 1:3500 catalysts. The HREM study of the Fe:Mn 3:1500 catalyst confirms the presence of two phases, the bixbyite and the Fe_xO_y. In Fig. 4a, an image with a bixbyite crystal is shown. Fig. 4b exhibits an area where distances of 3.1, 5.1 and 4.8 Å are measured. These distances may be assigned to the (2 2 0) and (1 1 1) family planes of the Fe_2O_3 cubic phase, and (2 0 0) of the bixbyite phase, respectively. These results are in agreement with those obtained from XRD (Fig. 1). In addition, the composition of the samples measured by EDX analyses shows the presence of Fe, Mn, and O in areas smaller than 25 nm. This result may be explained by a Mn_2O_3–Fe_2O_3 solid solution or by the existence of a mixed oxide such as a spinel phase. The quantitative analyses carried out in several areas show that Fe:Mn 1:1 and Fe:Mn 1:3 catalysts are homogeneous and that the ratio Fe:Mn in both samples correspond with the nominal one while Fe:Mn 3:1 catalyst is heterogeneous and the same areas have a higher amount of Fe than the nominal.

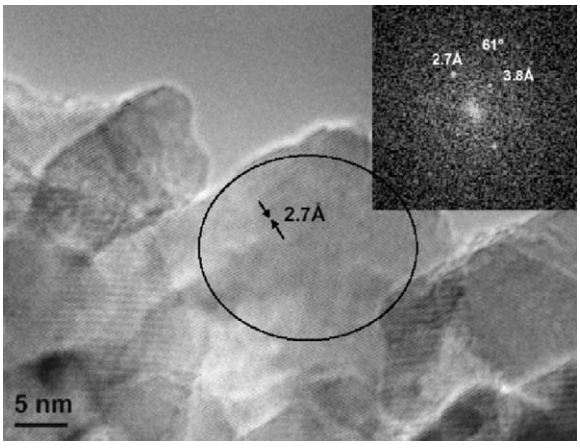

Fig. 3. HREM images of the FeMn 1:3500 catalyst.

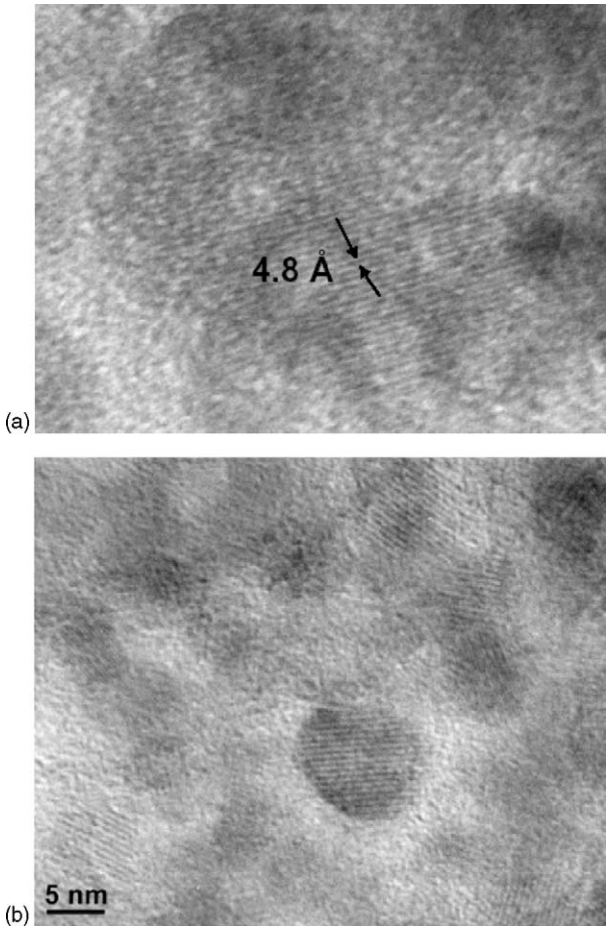

Fig. 4. HREM images of the FeMn 3:1500 catalyst.

The dissolution of Fe_2O_3 into α-Mn_2O_3 would change the Fe reducibility. The reducibility of the catalyst is a very important parameter which could explain the catalytic performance. In Fig. 5, the TPR profiles of all FeMn catalysts are compared to the TPR profiles of pure manganese and iron oxides as reference. The maximum of the major reduction peak of the FeMn mixed oxide catalysts is shifted towards higher temperatures suggesting that the mixed catalyst becomes more resistant to the reduction when Fe^{3+} is included in the Mn_2O_3 structure. The reduction to metallic ion occurs at 550–650 °C through an intermediate Wustite (FeO) phase. In the case of Mn–Fe oxide solid solution, the reduction of Fe^{3+} ion to Fe^{2+} may occur since the further reduction of Fe^{2+} to Fe^0 as expected on the basis of the standard reduction potential, will be very difficult. This ion behavior probably makes the mixed oxide more resistant to reduction. The unstable Wustite phase is stabilized by the inclusion of an appreciable amount of Mn^{2+} during reduction. These results are in agreement with those presented by Jaggi et al. [8].

However, the textural characteristic of the catalyst may also play an important role in the explanation of the catalytic performance (Fig. 6). A representative TEM image of the Fe:Mn 1:3500 shows, its morphology. In this image, it is difficult to measure the size of the crystals due to the overlap of the different contrasts. However, by HREM images of the sample, crystals can be clearly seen and measured (Fig. 3). Crystal sizes between 30 nm and 10 nm have been measured. The crystal sizes measured in HREM images of the other two samples are smaller—around 10 nm for FeMn 1:1 and between 10 and 8 nm for FeMn 3:1.

The degree of crystallinity of MnO_x is a key factor in the catalytic activity. TEM characterization shows that the average size of

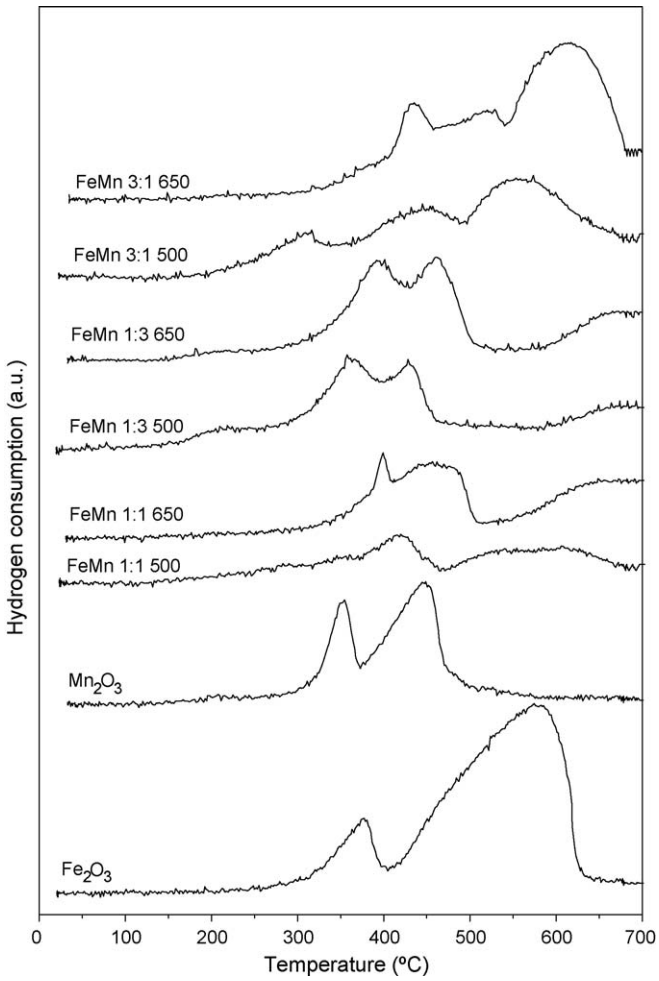

Fig. 5. Temperature programmed reduction profiles for mixed and pure oxides. Condition: sample weight: 0.045 g; reduction mixture: 5% H_2/N_2 at 30 ml min^{-1}; heating rate: 10 °C min^{-1} from 20 to 700 °C.

bixbyite crystals decreases significantly as Fe content increases. The sizes obtained from TEM measurements are 30–25, 25–10 and 10–8 nm for FeMn 1:3, 1:1 and 3:1, respectively. It is presumed that manganese is poorly crystalline in manganese poor catalysts [9]. With the increase of the calcination temperature or the manganese content, orthorhombic Mn_2O_3 transforms into cubic Mn_2O_3 via stabilization by the incorporation of Fe^{3+} ion in the lattice. It is likely that the particles of these oxide phases are too small to give well-defined XRD patterns. It is important to mention that, for FeMn 1:1500, FeMn 1:3500 and FeMn 3:1500 catalysts, the reduction in TPR experiments begins at lower temperatures than for the pure oxides. These signals at low temperatures may be assigned to the reduction of defective MnO_x species. The intensity of these signals increases in the following order: FeMn 3:1 < 500 < FeMn 1:3500 < FeMn 1:3650 catalysts. EDX analyses on FeMn 3:1500 catalyst show that when the Fe content is higher than the nominal values, small crystals of maghemite are also detected. From a rough evaluation of the unit cell parameters, Baldi et al. [5] show that Mn_2O_3 dissolution into α-Fe_2O_3 is likely of a few mol%. Beside the composition of the catalyst, the texture is very important in order to explain the catalytic performance. In TEM images (Fig. 7) contrasts associated with the presence of pores can be observed inside the crystals. The size of these pores decreases with the Fe content. Sizes in the ranges of 10–3, 6–3 and 4–2 nm have been measured for FeMn 1:3500, FeMn 1:1500, and FeMn 3:1500 catalysts, respectively. These results explain the high

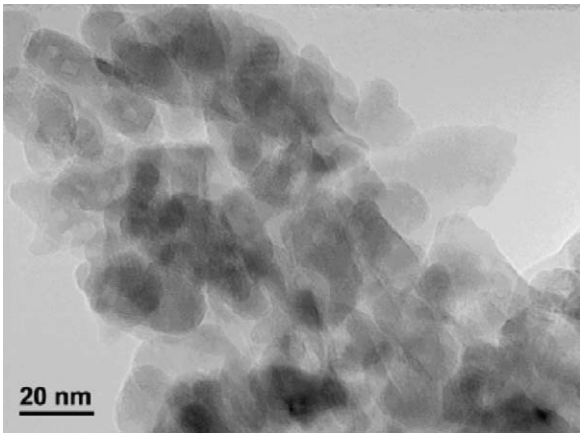

Fig. 6. Representative TEM image of the FeMn 1:3500 catalyst.

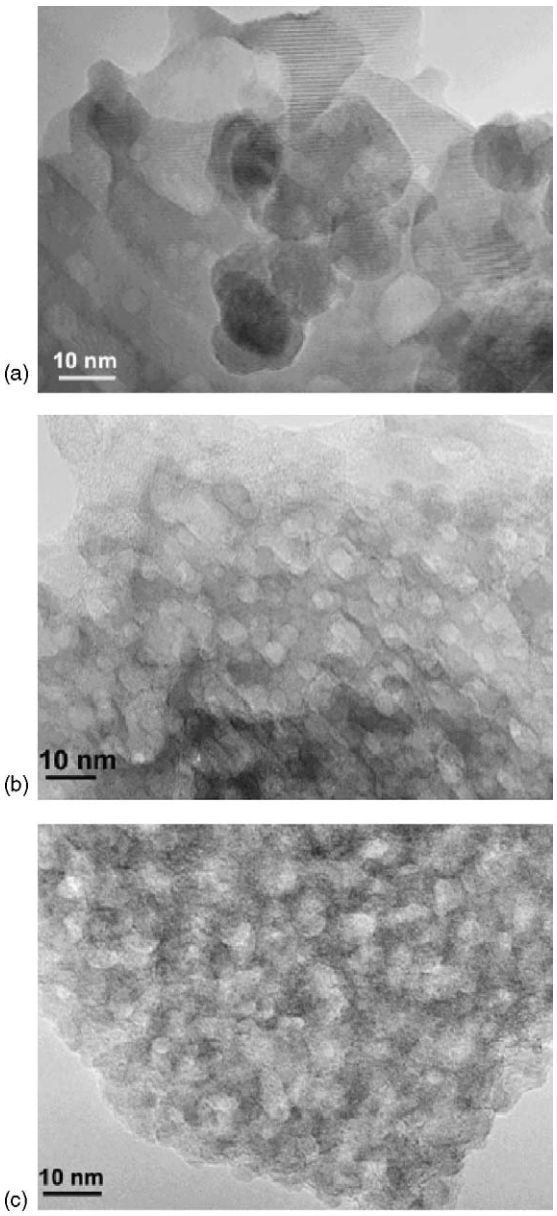

Fig. 7. TEM images inside the crystals for FeMn 1:3500, FeMn 1:1500 and FeMn 3:1500 catalysts.

Table 3
Specific surface areas by BET method (S_{BET}) and catalytic activity per surface area unit.

	Ethanol			Toluene	
	S_{BET}	Y_{220}	Y/S_{BET}	Y_{297}	Y/S_{BET}
FeMn 1:1500	85	82	0.97	85	1.00
FeMn 1:1650	30	30	1.00	33	1.10
	Ethanol			Toluene	
	S_{BET}	Y_{220}	Y/S_{BET}	Y_{282}	Y/S_{BET}
FeMn 1:3500	60	70	1.17	80	1.33
FeMn 1:3650	23	27	1.17	30	1.30

values of specific surface area obtained for the mixed oxides catalysts. S_{BET} values are directly related to the average size of the pore diameter (Table 2) and they indicate the catalyst sintering with the increase of the calcination temperature. Evidently, this sintering process is accompanied by an increase of the crystallinity.

3.1. Catalytic performance

The results of the catalytic evaluation in combustion of ethanol, ethyl acetate and toluene are shown in Table 1. FeMn 1:1500 catalyst is the most active. Its activity compared to Mn_2O_3 is relevant. The temperature corresponding total conversion is lowered 30 °C for ethanol combustion and about 25 °C for ethyl acetate combustion. In toluene combustion, the most active is FeMn 1:3500 catalyst and the T_{80} is lowered 14 °C.

The results of catalytic activity per surface area unit are shown in Table 3. These data are obtained by the simple division of the catalytic activity by the specific surface area. FeMn 1:1500 and FeMn 1:1650 catalysts have shown a value of approximately 1. The validity of these data obtained by a simple division was corroborated by an experimental procedure. Different catalyst mass were charged into the reactor with the aim of evaluating equals specific surface areas. The FeMn 1:3650 catalyst (300 mg) was used as reference. FeMn 1:3500, FeMn 1:1500 and FeMn 1:1650 catalysts mass were corrected. The discussion of catalytic performance will be focused on the ethanol and toluene combustion. Ethyl acetate was neglected due to the formation of ethanol as a partial product. The ethanol and ethyl acetate combustion could occur by a similar mechanism. Acetaldehyde was detected as partial oxidation product of ethanol. Acetaldehyde and ethanol were detected as partial oxidation products of ethyl acetate. Catalysts calcined at 500 °C showed T_{80} values slightly lower than that obtained for catalysts calcined at 650 °C. These results are coherent with a lower $\tau = W/F$ due to higher specific surface areas of the FeMn X:Y 500 catalysts. The results of catalytic activity per surface area unit are shown in Figs. 8 and 9.

TEM has shown that FeMn 1:1500 catalyst is extremely homogeneous in the $(FeMn)_2O_3$ phase. In this sense, FeMn 1:1500 catalyst may be used as reference of the $(FeMn)_2O_3$ catalytic phase. This catalyst shows an excellent catalytic performance in the combustion of all VOC molecules used in this work. When the specific conversion (defined as VOC conversion per surface area unit) is considered, the difference in activity is still observed. Thereby, it can be claimed that FeMn 1:3 T catalysts are the most active. The TPR profiles of FeMn 1:3650 and FeMn 1:3500 catalysts are very different from those of Mn_2O_3 and Fe_2O_3 pure oxides. A possible explanation for the easier manganese reduction in FeMn 1:3 catalysts in comparison with bulk Mn_2O_3 is the existence of structural defects associated with oxygen vacancies or with a high dispersion of Mn_2O_3 in the mixed phase. The structural defects associated with oxygen vacancies facilitate the catalyst

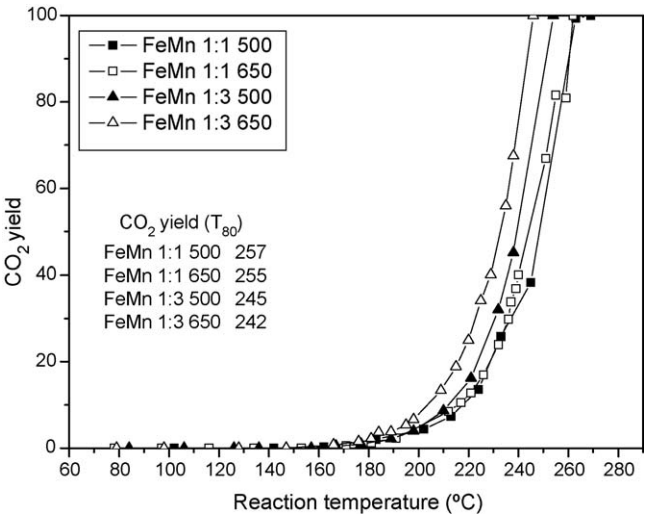

Fig. 8. Yield to CO_2 per surface area unit in the ethanol combustion.

reducibility [10]. This explains the enhancement of the catalytic activity. The catalytic performance in the ethanol combustion has the following order: FeMn 1:1500 = FeMn 1:1650 < FeMn 1:3500 < FeMn 1:3650. The amount of the manganese defective species may be estimated by means of the integrated area under the TPR curve between 200 and 320 °C. The catalytic activity and the manganese defective species amount follow the same order. However, toluene total oxidation shows that the T_{80} for FeMn 1:3500 is 282 °C which is 14 °C lower than the T_{80} of Mn_2O_3. In this reaction, the calcination temperature of the catalysts modifies the catalytic performance and as a consequence the T_{80} of toluene combustion is similar in all catalysts and approximately equal to that of Mn_2O_3. When the activity per surface area unit is considered (Fig. 8) the catalytic activity follows the order: FeMn 1:3650 > FeMn 1:1650 = FeMn 1:3500 > FeMn 1:1500. The enhancement of the catalytic performance with the increase of the calcination temperature of the catalysts, could be explained assuming that Mn_2O_3 migrates onto the surface achieving a high dispersion that facilitates its reduction. However, the atomic ratios obtained by XPS are not modified with the calcination temperature. At higher calcination temperature, the nature of the phases is not modified, although a variation in the relative intensity of diffraction lines is observed. Catalytic performance might be also attributed to the cooperation between both manganese and iron

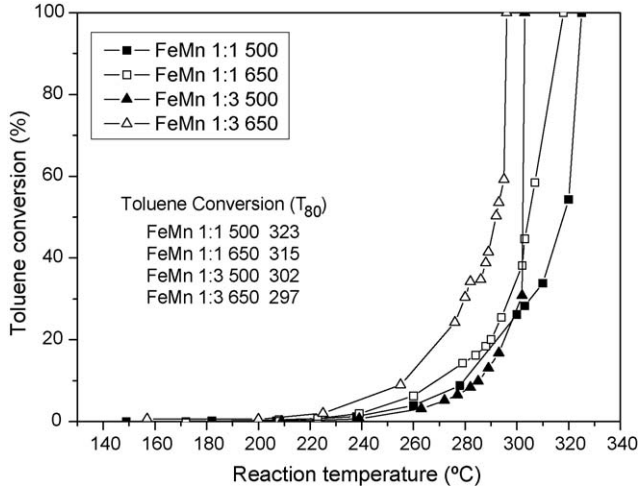

Fig. 9. Conversion of toluene per surface area unit.

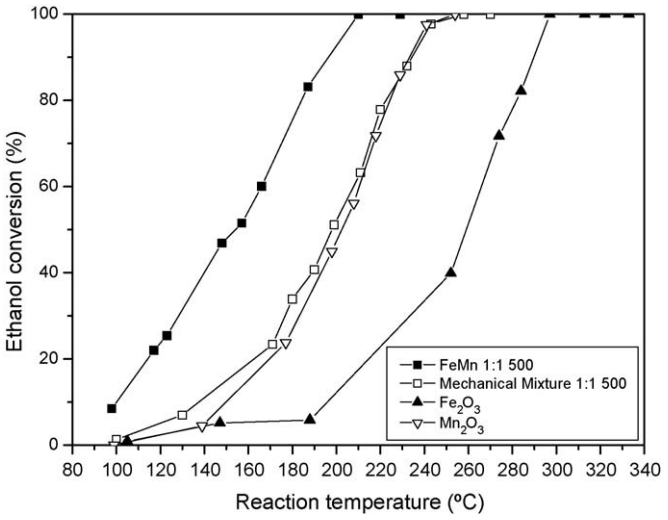

Fig. 10. Ethanol conversion as a function of the reaction temperature. Reaction conditions: catalyst weight = 300 mg; total volumetric flow = 100 ml min^{-1}; feed composition: $C_2H_5OH:O_2:He = 1:20:79$.

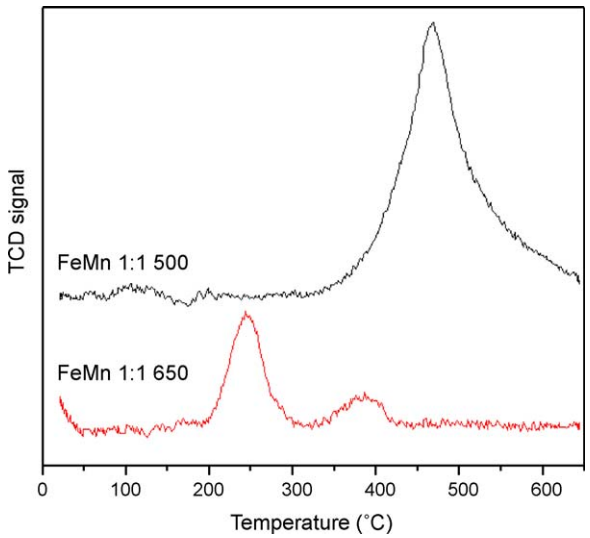

Fig. 11. O_2-TPD curves. Conditions: ample weight = 0.5 g; pre-treatment: helium pure (24 ml min^{-1}; 20–500 °C; 10 °C min^{-1}); cooling to room temperature and purge; desorption: helium pure (24 ml min^{-1}; 20–500 °C; 10 °C min^{-1}).

oxides, instead the solid solution formed. Trying to confirm the above, an artificially mechanical mixture was prepared. A 1:1 Mn_2O_3–Fe_2O_3 mechanical mixture was compared to the FeMn 1:1500 catalyst. Fig. 10 shows the results in the ethanol combustion. XRD analysis has shown that the mechanical mixture is formed by the two original phases. No new phases are formed.

The solid solution between Fe and Mn oxides has improved the catalytic performance with respect to the mechanical mixture of the pure oxides phases. T_{50} value is 150 and 200 °C respectively for FeMn 1:1500 and for the mechanical mixture. The T_{80} has a similar behavior.

In Fig. 10 both Mn_2O_3 and Fe_2O_3 catalytic performance are also included. The mechanical mixture has a behavior similar to those of Mn_2O_3. Baldi et al. [5] observed a similar catalytic result using Mn_2O_3–Fe_2O_3 mixed oxides prepared by co-precipitation. On the basis of this result, they proposed synergy between iron manganese components. Baldi et al. also observed that in Mn–Fe solid system prepared by co-precipitation method, Fe_2O_3 phase can achieve an approximate solubility of 30% in a-Mn_2O_3. Our catalyst, prepared by the citrate method, shows a high homogeneity as was described in Section 3.1. In addition, this catalyst was better than Mn_2O_3 catalyst. Evidently, the extension of the solid solution plays a key role in the enhancement of the catalytic activity.

Other factor extremely important is the existence of structural defects which are associated with oxygen vacancies. A useful technique to study oxygen vacancies is temperature programmed desorption of oxygen. Trawczynski et al. [11] observed desorption of oxygen at high temperature in supported manganese oxides. A peak between 524 and 590 °C was assigned to oxygen associated with defective MnO_x species. The O_2-TPD curve shows a desorption signal in the 147–427 °C range for FeMn 1:3 catalysts (Fig. 11) which may be assigned to oxygen species adsorbed on surface oxygen vacancies. These oxygen species (named as α-species) are very reactive and can improve notably the catalytic activity. Fig. 11 shows TPD of O_2 results. The amount of α-species of oxygen has the following the order FeMn 1:3650 > FeMn 1:3500 > FeMn 1:1650 > FeMn 1:1500. If the BET surface is taken into account, the amount of adsorbed oxygen species decrease in the following order: FeMn 1:3650 > FeMn 1:3500 = FeMn 1:1650 ≫ FeMn 1:1500. This is the same order as that observed for the activity per surface area unit and it may explain the catalytic performance in the combustion of toluene. The relationship between oxygen species and the catalytic activity indicates that these catalysts could activate hydrocarbon molecules, as toluene, in combustion processes by a Rideal Eley mechanism. Montes and co-workers [12] propose a similar mechanism for Pt catalysts.

FeMn 3:1500 catalyst is a heterogeneous catalyst and their catalytic performance can be explained as follows: (a) in ethanol combustion, it shows a poor performance due to the existence of Fe_2O_3 phase, but (b) in toluene combustion, due to the Rideal Eley mechanism, the higher concentration of MnO_x species compensates the presence of Fe_2O_3.

4. Conclusions

Considering the chemical, structural and textural characterization, it can be concluded that: (a) the citrate method is an appropriate method to prepare extremely homogeneous FeMn mixed oxide catalysts if the Fe:Mn atomic ratio does not exceed the tolerable Fe content for the formation of solid solution. (b) Fe^{3+} is included into the lattice of α-Mn_2O_3 a forming of a solid solution; at low temperature of calcination (500 °C) under the form of bixbyite (α-Mn_2O_3). For the low temperature form there are five distinguishable Mn-sites which may include great amounts of Fe. (c) $Mn_xFe_yO_4$ spinel existence is discarded. (d) The mixed catalysts become more resistant toward reduction when Fe^{3+} ions are present in the Mn_2O_3 structure. The reduction of Fe^{2+} does not occur below 700 °C, (e) when Mn is in excess, easily reducible defective MnO_x species are formed, (f) when the calcination temperature or the manganese content is increased, orthorhombic Mn_2O_3 transforms into cubic Mn_2O_3 via stabilization by the incorporation of Fe^{3+} ion in the lattice. Bixbyite crystal size decreases as the Fe content increases; (g) by the synthesis method, catalysts with high specific surface which has a direct relationship with the catalyst porosity can be obtained. When calcination temperature increases, catalysts synthesise and the size of crystals increases; (h) a better performance of FeMn 1:3650 in the ethanol and ethyl acetate combustion is associated with the existence of manganese defective species; (i) the higher calcination temperature favors a change in the crystallinity of the different phases forming the solid system. At higher calcinations temperature, the nature of the phases is not modified. However the existence of structural defects favors the adsorption of oxygen. These oxygen

species are very reactive and they improve notably the catalytic activity for toluene combustion.

Acknowledgements

The authors gratefully acknowledge Universidad Nacional de San Luis, CSIC-Spain/CONICET-Argentina, ANPCyT-Argentina and Junta de Andalucía for financial support.

References

[1] F.N. Agüero, A. Scian, B.P. Barbero, L.E. Cadús, Catal. Today 133–135 (2008) 493–501.
[2] M.A. Peluso, L.A. Gambaro, E. Pronsato, D. Gazzoli, H.J. Thomas, J.E. Sambeth, Catal. Today 133–135 (2008) 487–492.
[3] L. Lamaita, M. Peluso, J. Sambeth, H. Thomas, G. Meneli, P. Porta, Catal. Today 107–108 (2005) 133–138.
[4] M.I. Zaki, M.A. Hasan, L. Pasupulety, K. Kumari, Thermochim. Acta 303 (1997) 171–181.
[5] M. Baldi, V. Sanchez Escribano, J.M. Gallardo Amores, F. Milella, G. Busca, Appl. Catal. B: Environ. 17 (1998) L175–L182.
[6] H.H. Kedesdy, A. Tauber, J. Am. Ceram. Soc. 39 (1956) 425–431.
[7] S. Guillement-Fritsch, A. Navrotsky, P. Tailhades, H. Coradin, M. Wang, J. Solid State Chem. 178 (2005) 106–113.
[8] N.K. Jaggi, L.H. Schwartz, J.B. Butt, Appl. Catal. 13 (1985) 347–361.
[9] C.K. Das, N.S. Das, D.P. Choudhury, G. Ravichandran, D.K. Chakrabarty, Appl. Catal. A 111 (1994) 119–132.
[10] M.R. Morales, B.P. Barbero, L.E. Cadús, Appl. Catal. B 67 (2006) 229–236.
[11] J. Trawczynski, B. Bielak, W. Mista, Appl. Catal. B 55 (2005) 277–285.
[12] N. Burgos, M. Paulis, M.M. Antxustegi, M. Montes, Appl. Catal. B 38 (2002) 251–258.